

## HOT AND DENSE MATTER IN QUARK-HADRON MODELS\*

S. SCHRAMM, J. STEINHEIMER, P. RAU

FIAS, Goethe University Frankfurt  
Ruth-Moufang-Str. 1, 60438 Frankfurt am Main, Germany

*(Received January 2, 2012)*

In order to describe hot and dense matter in heavy-ion collisions as well as potentially in hybrid stars theoretical models have to include hadronic as well as quark degrees of freedom. We discuss a theoretical approach that treats quarks and hadrons in a unified way. We compare model results with lattice QCD calculations and discuss the phase diagram depending on temperature and chemical potential. In an extended study we investigate the SU(3) parity doublet model and show the properties of highly excited strongly interacting matter in such an approach.

DOI:10.5506/APhysPolBSupp.5.857

PACS numbers: 21.65.Mn, 12.38.Aw, 25.75.Nq

### 1. Introduction

The study of strongly interacting matter under extreme conditions is a central topic of modern nuclear and heavy-ion physics. Ultrarelativistic heavy-ion collisions allow for the creation of a short-lived fireball with high temperatures and, depending on the beam energy, varying net baryon density. On the other hand, compact stars have extremely dense cores, several times the value of nuclear matter saturation density, at low temperatures except for the first few seconds in the proto-neutron star phase, where temperature of about 30 MeV might be reached. For a description of these physical systems within a single approach, a unified model of the hadronic SU(3) degrees of freedom as well as quarks and gluons is needed. We discuss a model of this type, coupling a hadronic model with a PNJL type formulation for quarks. Such an approach allows for a very good description of nuclear properties as the hadronic model has been developed for just this purpose, and it automatically contains the correct degrees of freedom

---

\* Talk presented at HIC for FAIR Workshop and XXVIII Max Born Symposium “Three Days on Quarkyonic Island”, Wrocław, Poland, May 19–21, 2011.

at low and high temperatures and densities, respectively. The fact that the approach is unified and does not consist of two separate models for the hadronic and quark world allows for first-order phase transition as well as continuous cross-over phase transitions to be described.

## 2. The hadronic model

The hadronic SU(3) model incorporates the lowest SU(3) multiplets for baryons and mesons (see [1,2] for details). In the case of mean field approximation the equations read

$$L = L_{\text{kin}} + L_{\text{int}} + L_{\text{meson}}, \quad (1)$$

where  $L_{\text{int}}$  represents the interactions of the baryons and mesonic fields

$$L_{\text{int}} = - \sum_i \bar{\psi}_i [\gamma_0 (g_{i\omega} \omega + g_{i\phi} \phi) + m_i^*] \psi_i \quad (2)$$

with the non-strange and strange vector mesons  $\omega$  and  $\phi$ . Here, we assume isospin symmetric matter. In calculations of neutron stars, for example, also isovector fields are taken into account. The effective baryon mass  $m_i^*$  is given by

$$m_i^* = g_{i\sigma} \sigma + g_{i\zeta} \zeta + \delta m_i \quad (3)$$

including couplings to the non-strange and strange scalar fields  $\sigma$  and  $\zeta$  plus a small explicit mass term. The mesonic self-interactions are contained in  $L_{\text{mesons}}$ , which, in the case of the scalar fields, generates spontaneous chiral symmetry breaking. Self-interaction terms of vector fields and an explicitly chiral symmetry breaking term are included as well

$$\begin{aligned} L_{\text{meson}} = & -\frac{1}{2} (m_\omega^2 \omega^2 + m_\phi^2 \phi^2) - g_4 \left( \omega^4 + \frac{\phi^4}{4} + 3\omega^2 \phi^2 + \frac{4\omega^3 \phi}{\sqrt{2}} + \frac{2\omega \phi^3}{\sqrt{2}} \right) \\ & + \frac{1}{2} k_0 (\sigma^2 + \zeta^2) - k_1 (\sigma^2 + \zeta^2)^2 - k_2 \left( \frac{\sigma^4}{2} + \zeta^4 \right) - k_3 \sigma^2 \zeta \\ & + m_\pi^2 f_\pi \sigma + \left( \sqrt{2} m_k^2 f_k - \frac{1}{\sqrt{2}} m_\pi^2 f_\pi \right) \zeta \\ & + \chi^4 - \chi_0^4 + \ln \frac{\chi^4}{\chi_0^4} - k_4 \frac{\chi^4}{\chi_0^4} \ln \frac{\sigma^2 \zeta}{\sigma_0^2 \zeta_0}. \end{aligned} \quad (4)$$

The dilaton field  $\chi$  represents the gluon condensate in the system [2]. The masses of the baryons are generated by the non-vanishing scalar condensates in the vacuum.

In Fig. 1 the phase diagram of the model is shown if one also includes higher resonances. In this specific calculation the effect of these resonances beyond the lowest baryonic octet were mimicked by a test resonance with a specific mass and degeneracy that couples to the fields [3]. For a large vector coupling constant the phase diagram does not show a first-order phase transition (except for the liquid–gas phase transition). If one wants to reproduce the critical end point in the phase diagram as originally determined in Ref. [5], a rather low value for the coupling  $g_V^R = 0.4$  (in units of the nucleon–omega vector coupling) is required. With this (purely hadronic) model one can determine the isotropes for fixed entropy per baryon, corresponding to different beam energies, starting from conditions of the fireball estimated in a simple overlap estimate. In a more microscopic approach, one can generate initial conditions for a given beam energy in a UrQMD cascade calculation and then perform a hydrodynamical evolution with the Equation of State from the model just described. Both approaches yield similar results as shown in Fig. 2.

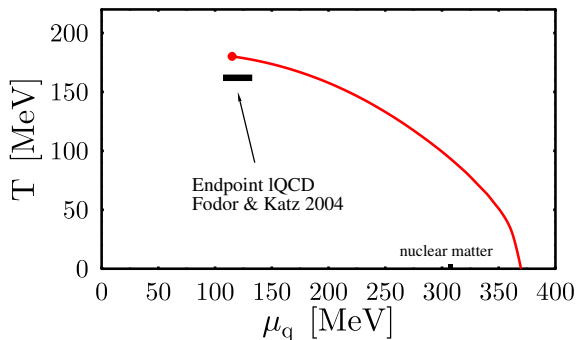


Fig. 1. Phase diagram of the hadronic model including test resonance in the  $T$ – $\mu_q$  plane. A line of first-order chiral phase transition with critical end point is shown [4]. A lattice prediction for the end point is indicated in the plot [5].

While the figure shows that a beam energy of 160 A MeV is best suited to reach the predicted critical end point, in a microscopic calculation one automatically has a distribution of temperature and chemical potentials in the dynamics of the hydrodynamical evolution that can be extracted from the propagated densities and energy densities. Therefore, also other beam energies will sample the critical region. In quantitative terms this is shown in the right panel of Fig. 2. The curves indicate the amount of the system that has values  $T_c - 10 \text{ MeV} \leq T \leq T_c + 10 \text{ MeV}$  and  $\mu_c - 10 \text{ MeV} \leq \mu \leq \mu_c + 10 \text{ MeV}$  as a function of time. One can see that a substantial volume is in the critical region at energies distinctly below and above 160 A GeV.

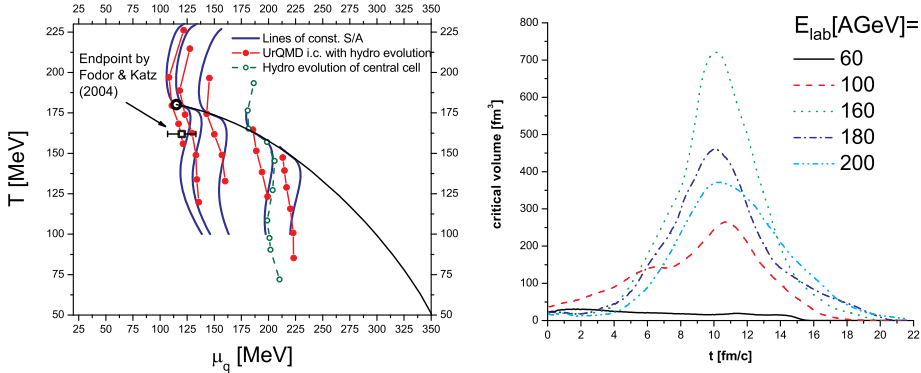


Fig. 2. Left: Isentropes (full lines) for the evolution of the system with fixed  $S/A$  ratio. The isentropes correspond to Pb+Pb beam energies (from right to left) of 5, 10, 40, 100, and 160 AGeV, respectively. The lines with circles show the corresponding results using UrQMD initial conditions and subsequent hydrodynamical evolution (see [6]). Right: Volume of the system with  $T, \mu$  parameters close to the critical end point as function of collision time for different beam energies [6].

In a related investigation, we treat all particles of the particle data group listings up to a mass of 2.6 GeV in the same manner as the lowest multiplets [7]. The vector coupling is varied in a similar way as in Fig. 1. The result shows a developing critical first-order chiral transition line at high chemical potentials with decreasing coupling strength. Note that for large values of  $T_c$  and small values of  $\mu_c$ , respectively, the phase transition at vanishing temperature occurs at lower densities as the liquid–gas transition, with the result that the normal nuclear matter ground state does not exist anymore.

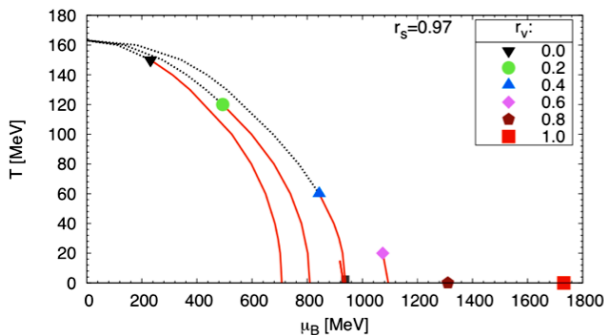


Fig. 3. Phase diagram of the hadronic SU(3) model including all known hadronic resonances up to 2.6 GeV. The critical transition line vanishes with increasing relative vector interaction strength  $r_v$  of the resonances.

### 3. Quarks and hadrons

In addition, the model contains quark degrees of freedom that couple linearly to the mean fields together with a Polyakov loop  $\Phi$  field that serves as the order parameter for deconfinement in the spirit of the PNJL model for quarks [8, 9]. We adopt a standard choice of an effective potential for the Polyakov loop [9]

$$U = -\frac{1}{2}a(T)\Phi\Phi^* + b(T)\ln\left[1 - 6\Phi\Phi^* + 4(\Phi^3\Phi^{*3}) - 3(\Phi\Phi^*)^2\right] \quad (5)$$

with  $a(T) = a_0T^4 + a_1T_0T^3 + a_2T_0^2T^2$ ,  $b(T) = b_3T_0^3T$ , where the constants are taken from [9]. In some calculations we considered the impact of changing the temperature scale  $T_0$  from its quenched value of 270 MeV to a smaller value, in our case 220 MeV.

The quarks and antiquarks couple to the effective Polyakov loop field  $\Phi$  as order parameter of the deconfinement phase transition like

$$\Omega_q = -T \sum_{i \in Q} \frac{\gamma_i}{(2\pi)^3} \int d^3k \ln \left( 1 + \Phi \exp \frac{E_i^* - \mu_i^*}{T} \right) \quad (6)$$

with a corresponding expression for the antiquarks [10]. In effect, we combine a hadronic model with a quark PNJL model (a detailed discussion can be found in [10]). In order to naturally suppress hadrons at high densities and temperatures, we take into account an excluded volume correction in a thermodynamically consistent manner as described in [10, 11, 12]. For an alternative way to formulate the HQM model and to suppress hadrons at high temperatures see [13].

Figure 4 shows the comparison of the model result for the energy density and pressure at vanishing chemical potential with results from lattice simulations [14]. One can see a reasonable agreement, where at lower temperatures the model calculation shows higher values, which is in accordance with the fact that the lattice simulations most likely do not contain an accurate description of the hadronic resonance gas, which dominates the low  $T$  region.

Studying the phase structure of this quark-hadron (QH) model we obtain the result as shown in the right panel of Fig. 4. Here the dependence of the scalar condensate  $\sigma$  is shown as a function of temperature and quark chemical potential. By construction, the first-order nuclear liquid–gas phase transition is retained. In general, the chiral restoration develops smoothly without a further critical end point. Also shown is the peak in the temperature derivative of the Polyakov loop indicating position of the deconfinement transition as measured by  $\Phi$ . As in the PNJL calculations this transition is

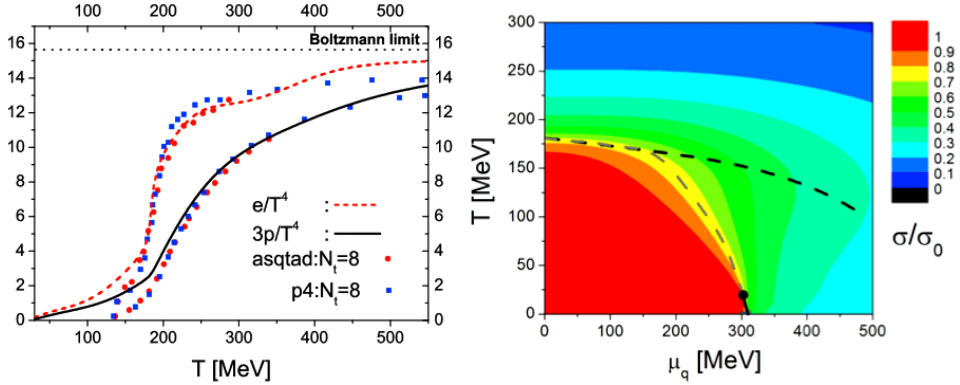


Fig. 4. Left: Energy density and pressure normalized by  $T^4$  as function of temperature compared to lattice QCD results. Right: Values of the non-strange scalar condensate as function of temperature and quark chemical potential. The liquid–gas first-order transition line is indicated that is continued as cross-over for higher temperatures. The values of the cross-over transition of the Polyakov loop are also indicated as upper dashed line [10].

rather independent of  $\mu$ . However, this behavior drastically changes, when the Polyakov loop potential depends explicitly on the chemical potential as we have discussed in [13].

A number of quark model calculations include relatively strong repulsive quark vector interactions, for instance PNJL models with large vector coupling generate relatively large  $T_c$  values for the critical end point. The same is true for many hybrid star calculations stabilizing a large quark core. In that case, a repulsive quark interaction stiffens the Equation of State generating higher neutron star masses. Using such parameterization for vanishing or small chemical potential the behavior of the pressure as a function of  $\mu$  is substantially modified. This leads to very different values of the Taylor coefficients  $c_n$  defined by

$$c_n(T) = \frac{1}{n!} \left. \frac{\partial^n (p(T, \mu_B)/T^4)}{\partial (\mu_B/T)^n} \right|_{\mu_B=0}. \quad (7)$$

Figure 5 illustrates the impact of the vector coupling on  $c_2$ . One can see that in the PNJL approaches as well as in the QH model an increase of the coupling strongly suppresses  $c_2$  at higher temperature in clear contradiction to lattice QCD [15, 16].

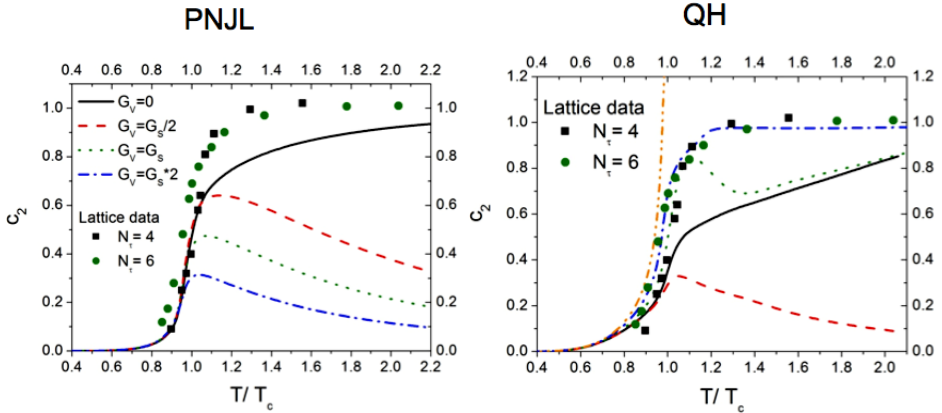


Fig. 5. Left:  $c_2$  Taylor expansion parameter as function of temperature in a PNJL calculation. The value of the quark vector coupling is modified showing a substantial change of  $c_2$  above  $T_c$  [16]. Right: Same as left figure performed in the QH model. A similar behavior as in the PNJL model can be observed.

#### 4. Results for the SU(3) parity model

In an analogous approach as in the previous section we study the behavior of the quark-hadron model in the case of the parity-doubling realization of chiral symmetry. We extend previous flavor-SU(2) investigations [17, 18, 19, 20, 21] to SU(3). Here we take into account the baryonic octet as well as the octet of the baryons with opposite parity [22] following [23]. In the case of the nucleon, an obvious candidate of a parity-doublet partner is the  $N(1535)$ . However, the actual state could also be a broad structure in the corresponding spectral density. For the hyperons, candidates are  $\Lambda(1670)$  and  $\Sigma(1750)$ . In the  $\Xi$  channel the experimental situation is very unclear. Within such an approach it is possible to define a mass-like term that couples the two multiplets  $\varphi_-$  and  $\varphi_+$  and their left- and right-handed components (L/R), which reads schematically (for more details, see [22])

$$m_0(\bar{\varphi}_- \gamma_5 \varphi_+ - \bar{\varphi}_+ \gamma_5 \varphi_-) = m_0(\bar{\varphi}_- \text{L} \varphi_+ \text{R} - \bar{\varphi}_- \text{R} \varphi_+ \text{L} - \bar{\varphi}_+ \text{L} \varphi_- \text{R} + \bar{\varphi}_+ \text{R} \varphi_- \text{L}), \quad (8)$$

where  $m_0$  represents a mass parameter.

After diagonalization the effective mass of baryon  $i$  reads

$$m_{i\pm}^* = \sqrt{\left[ \left( g_{\sigma i}^{(1)} \sigma + g_{\zeta i}^{(1)} \zeta \right)^2 + (m_0 + n_s m_s)^2 \right] \pm g_{\sigma i}^{(2)} \sigma \pm g_{\zeta i}^{(2)} \zeta}, \quad (9)$$

where the various coupling constants of baryons and scalar mesons  $g_{\sigma i}^{(j)}, g_{\zeta i}^{(j)}$  are connected via SU(3) relations [22].  $m_s$  is the strange quark mass and  $n_s$  denotes the number of strange quarks of the corresponding baryonic state.

Varying the mass of the nucleonic parity partner one obtains the behavior of the scalar condensate field  $\sigma$  as a function of chemical potential for  $T = 0$  as shown in Fig. 6. There is a transition between a first-order transition for masses larger than about 1460 MeV and a smooth cross over at lower values.

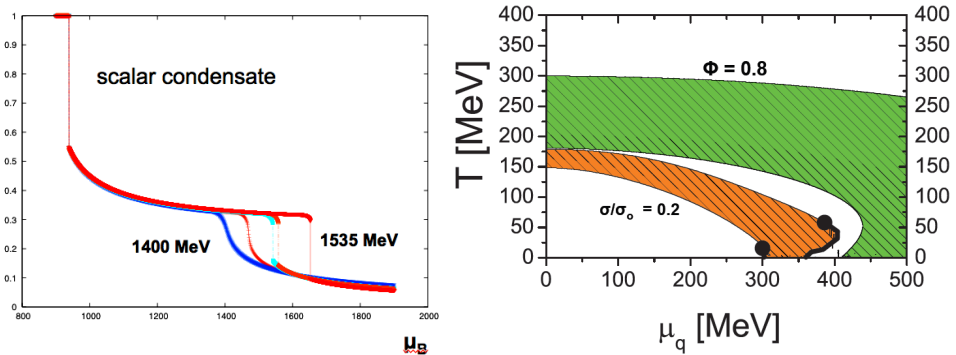


Fig. 6. Left: Dependence of the scalar field as a function of baryochemical potential at  $T = 0$ . Results for different values of the mass of the nucleonic parity partner is shown. In result of lowering the mass, the chiral transition switches from first-order to a cross-over [24]. Right: Behavior of the deconfinement parameter  $\Phi$  and the scalar condensate  $\sigma$  in the  $T - \mu_q$  plane. Two first-order phase transition lines with corresponding critical end-points can be observed. The marked regions are discussed in the text.

When scanning the whole range of temperatures and chemical potentials we obtain the phase structure of this approach, shown in the right panel of Fig. 6. The region of the chiral restoration, where the value of the scalar condensate ranges between 20 and 80 percent of its vacuum value is shown in light gray (orange) and, correspondingly the area, where the Polyakov loop has a value between 0.2 and 0.8 is shown in dark gray (green). There are two first-order transition lines, the liquid–gas transition and a further chiral transition, where baryonic parity partners and quarks begin to be populated. The general structure of the phase transitions resembles the behavior suggested in the quarkyonic picture of chiral and deconfinement transitions [25]. At zero chemical potential the comparison to lattice results indicates a reasonable agreement with the lattice data. In the upper left panel of Fig. 7 the rise of the Polyakov loop value with temperature is shown. Results for two different values of the potential parameter  $T_0$  are shown. A lower value of  $T_0$  of 220 MeV agrees quite well with the slow rise of the Polyakov loop as observed on the lattice. The corresponding results for the quark condensate are shown in the upper right panel. The lower right panel depicts the so-called interaction measure  $\epsilon - 3p$  divided by  $T^4$ . The population of different particle species as a function of temperature

can be seen in the lower-right panel. Since the temperature dependence of the Polyakov loop, as measured on the lattice, indicates a slow transition [26, 27], a larger temperature range with a mixed phase of hadrons and quarks is a quite natural assumption. This is also the behavior observed in our model with appreciable hadronic contributions up to temperatures of around 300 MeV.

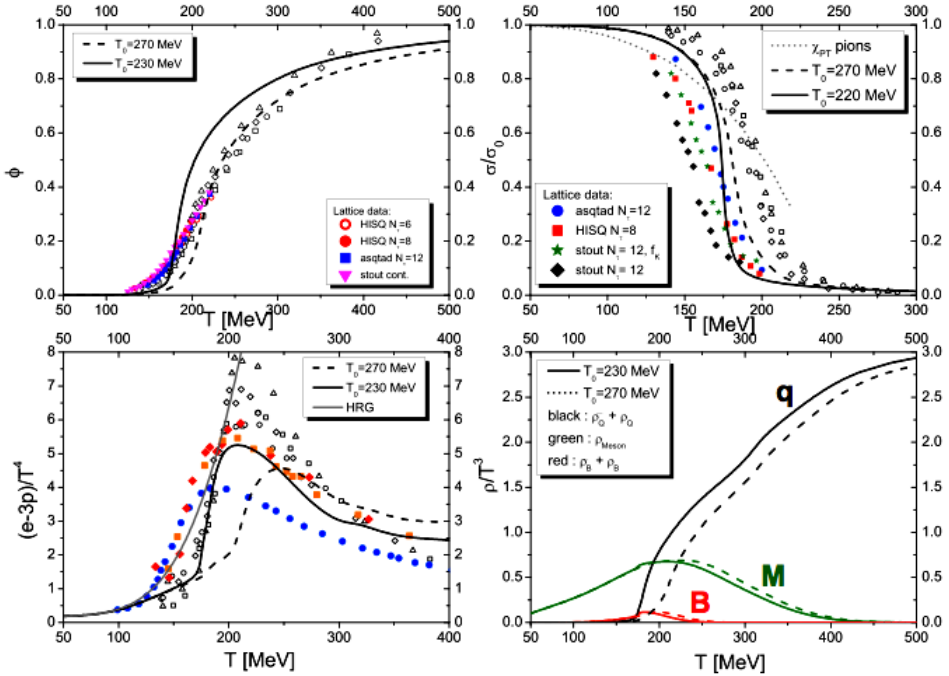


Fig. 7. Results of the SU(3) parity model for vanishing chemical potential. In the upper row the Polyakov loop and the scalar condensate are compared to lattice results. The lower row shows the interaction measure  $(\epsilon - 3p)/T^4$  and the densities of baryons, mesons, and quarks as function of temperature.

## REFERENCES

- [1] P. Papazoglou *et al.*, *Phys. Rev.* **C57**, 2576 (1998).
- [2] P. Papazoglou *et al.*, *Phys. Rev.* **C59**, 411 (1999).
- [3] D. Zschesche, G. Zeeb, S. Schramm, H. Stoecker, *J. Phys. G* **31**, 935 (2005).
- [4] D. Zschesche, G. Zeeb, S. Schramm, *J. Phys. G* **34**, 1665 (2007).
- [5] Z. Fodor, S.D. Katz, *J. High Energy Phys.* **0404**, 050 (2004).

- [6] J. Steinheimer *et al.*, *Phys. Rev.* **C77**, 034901 (2008).
- [7] P. Rau, J. Steinheimer, S. Schramm, H. Stöcker, *Phys. Rev.* **C85**, 025204 (2012) [arXiv:1109.3621v3 [hep-ph]].
- [8] K. Fukushima, *Phys. Lett.* **B591**, 277 (2004).
- [9] C. Ratti, M.A. Thaler, W. Weise, *Phys. Rev.* **D73**, 014019 (2006).
- [10] J. Steinheimer, S. Schramm, H. Stöcker, *J. Phys. G* **38**, 035001 (2011).
- [11] D.H. Rischke, M.I. Gorenstein, H. Stoecker, W. Greiner, *Z. Phys.* **C51**, 485 (1991).
- [12] J. Cleymans, M.I. Gorenstein, J. Stalnacke, E. Suhonen, *Phys. Scr.* **48**, 277 (1993).
- [13] V.A. Dexheimer, S. Schramm, *Phys. Rev.* **C81**, 045201 (2010).
- [14] A. Bazavov *et al.*, *Phys. Rev.* **D80**, 014504 (2009).
- [15] M. Cheng *et al.*, *Phys. Rev.* **D79**, 074505 (2009).
- [16] J. Steinheimer, S. Schramm, *Phys. Lett.* **B696**, 257 (2011) [arXiv:1005.1176 [hep-ph]].
- [17] C.E. Detar, T. Kunihiro, *Phys. Rev.* **D39**, 2805 (1989).
- [18] D. Zschesche, L. Tolos, J. Schaffner-Bielich, R.D. Pisarski, *Phys. Rev.* **C75**, 055202 (2007).
- [19] V. Dexheimer, S. Schramm, D. Zschesche, *Phys. Rev.* **C77**, 025803 (2008).
- [20] V. Dexheimer *et al.*, *Eur. Phys. J.* **A38**, 105 (2008).
- [21] C. Sasaki, I. Mishustin, *Phys. Rev.* **C82**, 035204 (2010).
- [22] J. Steinheimer, S. Schramm, H. Stöcker, *Phys. Rev.* **C84**, 045208 (2011) [arXiv:1108.2596v1 [hep-ph]].
- [23] Y. Nemoto, D. Jido, M. Oka, A. Hosaka, *Phys. Rev.* **D57**, 4124 (1998).
- [24] S. Schramm, V. Dexheimer, R. Negreiros, J. Steinheimer, arXiv:1110.0609v1 [nucl-th].
- [25] L. McLerran, R.D. Pisarski, *Nucl. Phys.* **A796**, 83 (2007).
- [26] S. Borsanyi *et al.*, *J. High Energy Phys.* **1011**, 077 (2010).
- [27] A. Bazavov, P. Petreczky [HotQCD Collaboration], *J. Phys. Conf. Ser.* **230**, 012014 (2010).